NANO: Brief Reports and Reviews
Vol. 15, No. 2 (2020) 2050016 (8 pages)

DOI: 10.1142/S1793292020500162

World Scientific
www.worldscientific.com

Manufacturing and Characterization on a Three-Dimensional Random Resonator of Porous Silicon/TiO_2 Nanowires for Continuous Light Pumping Lasing of Perovskite Quantum Dots

Yining Mu*, Tuo Zhang*, Tianqi Chen*, Fanqi Tang*, Jikai Yang*,‡, Chunyang Liu*, Zhangxiaoxiong Chen*, Yiming Zhao*, Peng Du*, Haibo Fan*, Yan Zhu*, Guozhen Liu* and Ping Li†,§

*Changchun University of Science and Technology
Changchun, Jilin 130022, P. R. China

†Changchun University of Finance and Economics
Changchun, Jilin 130122, P. R. China
‡muyining1985@hotmail.com
§liping_1958@163.com

Received 30 October 2019
Accepted 11 December 2019
Published 11 February 2020

In recent years, all inorganic bismuth lead-halide perovskite nanocrystals [$CsPbX_3$ (X = Cl, Br, I)] have received extensive attention due to their high performance in fluorescence quantum yield, narrow emission spectrum, and adjustable emission range. However, the disadvantages of high cost and poor stability have greatly limited the development prospects of the material. Here, in order to develop a perovskite quantum dot lasing cavity with high chemical stability, high quality factor and low fabrication cost, we have successfully fabricated a 3D random cavity device based on porous silicon/TiO_2 nanowires. A TiO_2 nanowire is grown on the porous silicon to form a 3D resonant cavity, and a perovskite quantum dot is spin-coated on the surface of the 3D resonant cavity to form a novel 3D complex film. The novel structure enhances the chemical stability and lasing quality factor of the resonant cavity while the fluorescence generated by the large quantum dots in the spatial interference structure constitutes the feedback loop, which will provide favorable support for the development of information optics.

Keywords: Perovskite quantum dots; porous silicon; TiO_2; resonators.

1. Introduction

The all-inorganic bismuth-lead halide perovskite material has been favored widely by researchers at home and abroad in recent years, relying on its own high quantum yield, low lasing threshold and fine transient optical properties.[1–5] Especially based on $CsPbX_3$ (X = I, Br, Cl) system of quantum dots,[6,7] one-dimensional (1D) nanowires,[8–11] two-dimensional (2D) nanoplates[12–15] and other microstructures, optical pump lasing,[16,17] electroluminescence (EL),[18–20] spontaneous radiation,[21] photoelectric detector,[22] X-ray detector,[23] light emitting diode[24] and other domains have achieved more and better results. However, as a halide, not only the different

‡,§Corresponding authors.

dimensional resonators formed by $CrsPbX_3$ (X = I, Br, Cl) are difficult to manufacture and more expense, but also the device failure rate of these micro-nano resonance mechanisms is much faster than its own films, which means that the quality of these halide resonant structures is changing with time. To this end, it is necessary to develop a stable and efficient resonant cavity for the perovskite material system.

In this paper, the fabrication of 1D TiO_2 nanowires on a 2D substrate of porous silicon (porous Si) to form a 3D resonant cavity is proposed. Spin-coating a perovskite quantum dot on the surface of the 3D resonant cavity not only greatly increases the probability that the fluorescence emitted by the quantum dot constitutes a feedback loop in the spatial interference structure, but also effectively improves the chemical stability and lasing quality factor of the resonant cavity.

2. Preparation and Characterization of Porous Si

In this paper, porous Si is prepared by metal-assisted chemical etching using two-step etching. These two steps are the deposition of precious metal catalytic particles on the surface of the silicon wafer and the oxidative etching of the surface of the silicon wafer. In the deposition process, silver particles are used as catalysts. The specific flow diagram is shown in Fig. 1. A silicon wafer is firstly immersed in a deposition solution mixed with $AgNO_3$ and HF [Fig. 1(a)], which can let silver elemental particles deposited on the surface of the silicon wafer and produce a Schottky barrier in the region where the silver particles contact the silicon wafer [Fig. 1(b)]. Next, the silicon wafer with silver particles is placed in an etching solution containing an oxidant and HF in order to etch a pore-shaped structure [Fig. 1(c)] at the position where the surface of the silicon wafer contacts the silver particles. Finally, the porous silicon is obtained by removing the silver particles [Fig. 1(d)].

In a mixed solution of silver nitrate and hydrofluoric acid, elemental silver particles will contact the surface of the silicon wafer to form a Schottky barrier. Subsequently, the corresponding barrier layer can be removed by a mixed etching solution of an oxidizing agent and hydrofluoric acid to form a corresponding etched porous structure. The morphology of porous silicon is mainly determined by the silver particles deposited on its surface. Because of there being the obvious cluster effect of silver particles, with the increase of etching time, the number of silver particles will increase and the cluster effect will be more obvious, which immediately leads to larger pores on the surface of porous silicon and affect its morphology. When the silver particles are relatively dense, the linear structure is etched.[25] The specific principle is shown in Fig. 2.

The specific formulation of manufacturing porous silicon in this paper is shown in Table 1.

The surface of the sample of Table 1 is characterized by SEM image. The specific contrast effect is shown in Fig. 3. With the increase of etching time, the surface pore size of porous silicon samples is gradually increased. However, because of there being anisotropy in metal-assisted chemical etching, in the initial stage of etching, silver particles will randomly etch in all directions and form irregular

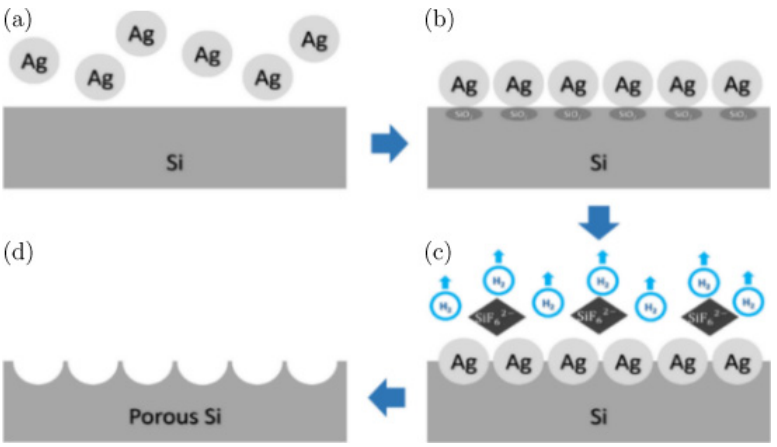

Fig. 1. Process of preparing porous Si by metal-assisted chemical etching.

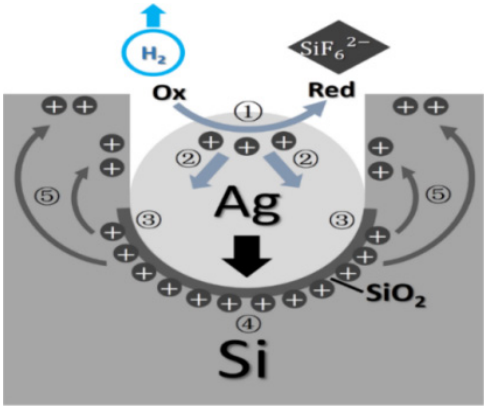

Fig. 2. Mechanism diagram of preparation of porous Si by metal-assisted chemical etching.

Table 1. Numbers and parameters for preparing different porous silicon samples.

No.	$AgNO_3$ (mol/L)	HF(mol/L)	H_2O_2 (mol/L)	Reflection time (min)
1-1	0.01	4.65	0.5	**15**
1-2	0.01	4.65	0.5	**25**
1-3	0.01	4.65	0.5	**35**
1-4	0.01	4.65	0.5	**45**

structures. For example, the edge of the pores of porous silicon samples becomes relatively smooth due to the clustering of irregular silver particles, so the roughness of samples 1-3 is higher than that of samples 1-4.

3. Preparation and Characterization of Porous Si/TiO_2 Complex Films

Due to the lattice mismatch between Si and TiO_2, it is difficult to directly grow high-quality TiO_2 nanowires on the porous silicon surface by hydrothermal method. In order to solve this problem, we firstly make a seed layer on the surface of porous Si. The specific steps are as follows: The polytetrafluoroethylene (PTFE) frame with porous silicon was immersed in a beaker containing the seed layer solution for 2 min, then taken out, and immersed in ethanol for 1 min; the porous Si and the PTFE frame were blown together using nitrogen gas. Finally, the sample was taken off and placed on a quartz boat and placed in a tube furnace, and annealed at a temperature of 500°C for 2 h without rare gas protection to complete the preparation of the seed layer. Subsequently, in order to complete the preparation of the complex film, we placed the porous Si sample in a hydrothermal kettle PTFE liner while fixing the tilted sample with a PTFE block, and then poured 15 mL of the precursor solution to make the solution and immersed the sample to reach 70% of the volume of the PTFE liner. Then, we placed each hydrothermal kettle with the same sample in a blast drying oven preliterated to 150°C for 6 h, took out the sample and rinsed with deionized water, and then annealed the sample at 450°C for half an hour. The specific parameters of our sample preparation are shown in

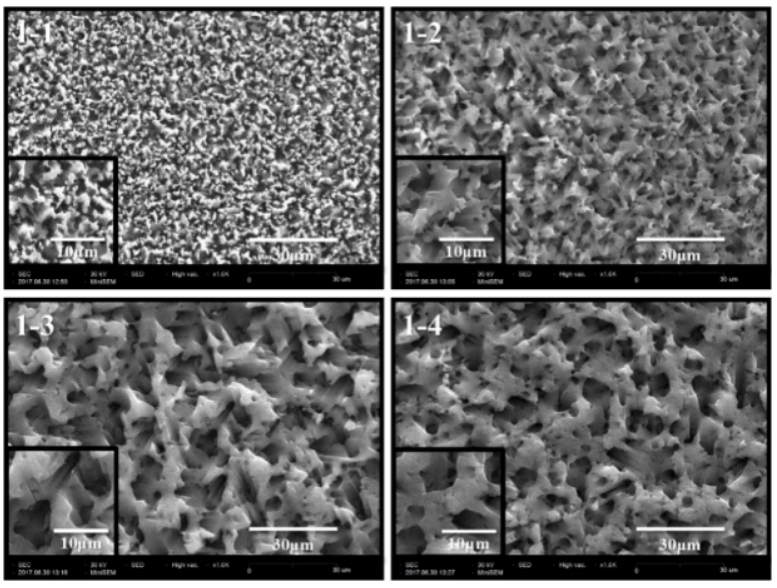

Fig. 3. SEM characterization of porous Si samples.

Table 2, and the corresponding SEM characterization results of the same porous Si/TiO_2 complex film samples are shown in Fig. 4. Because of the smaller pore structure of the complex film samples 3-1 and 3-2, the pore may be completely covered by TiO_2 nanowires, which makes it difficult for perovskite quantum dots to be filled in. On the contrary, the etching time of sample 3-3 and sample 3-4 is longer, which makes the pore size of porous silicon surface larger, and is very conducive to the subsequent implantation of quantum dots. In addition, due to the rougher surface of the 3-3 pore structure of the sample, the growth of TiO_2 nanowires will be more conducive to lasing with subsequent perovskite quantum dots.

In order to determine the crystal composition of the porous Si/TiO_2 complex film sample, we performed an XRD test on the light sample 3-3, and the test results are shown in Fig. 5. It can be seen from the figure that the porous Si/TiO_2 complex film sample has a very distinct Si <111> (JCPDF No. 78-2500) diffraction peak at $2 = 28.4°$, and the rutile phase TiO_2 (Rutile) also appears in the spectrum. (JCPDF No. 02-0494) Diffraction peaks ($2 = 23°$, $33°$, $37°$, $39°$, $54°$, $64°$, $71°$), and anatase phase TiO_2 (Anatase) (JCPDF No. 02-0406) Diffraction peak ($2 = 21°$, $47°$), which indicates that the surface of the porous silicon is grown with a TiO_2 nanowire layer, and most of the TiO_2 is a rutile phase. According to the XRD diagram, there are three different diffraction peaks in the sample, so the

Table 2. Number and parameters of different porous Si/TiO_2 complex film photoanode samples.

No.	Etching time (minutes)	Growth time (h)
3-1	**15**	6
3-2	**25**	6
3-3	**35**	6
3-4	**45**	6

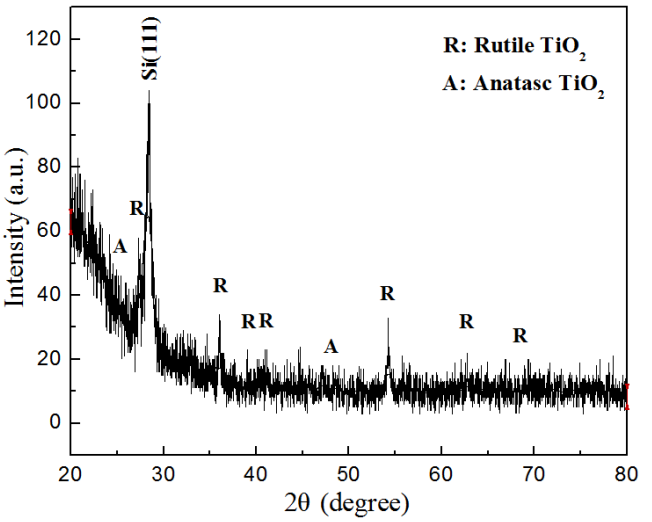

Fig. 5. XRD chart of porous Si/TiO_2 complex film samples.

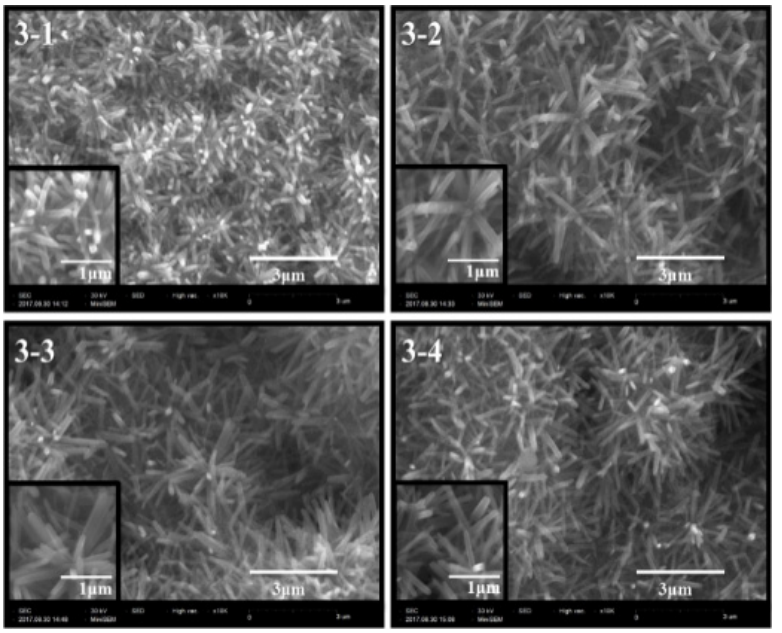

Fig. 4. SEM characterization of porous Si/TiO_2 complex film samples.

porous Si/TiO_2 complex film can be synthesized and characterized successfully.

4. Preparation of $CsPbBr_3$ Quantum Dots and Structural Characterization of 3D Complex Thin Films

According to the literature,[26,27] an excitation light can be generated by the particle beam inversion of $CsPbBr_3$ quantum dot thin film under shorter wavelength light pump model, and the excitation light will be randomly scattered in the $CsPbBr_3$ quantum dot thin film. When the scattering is strong enough, continuous multiple scattering may make the excitation light and photons return to the original scattering point and form a feedback loop by coherent superposition in space, which will have a great probability to form local resonance of light and produce random laser. Therefore, in order to verify the amplification ability of 3D random resonator to this random lasing, this paper used $CsPbBr_3$ quantum dot film as a luminescent material. The specific preparation process of the $CsPbBr_3$ quantum dot is as follows: as shown in Fig. 6.

First, the $CsPbBr_3$ quantum dot were synthesized by high-temperature thermal implantation and fast ion exchange in oil phase protected by inert gas using cesium oleate and lead bromide as precursors.

The concrete method is as follows: 0.0738 g of lead bromide and 10 mL of octadecene are weighed with an electronic balance, put into a 50 mL glass bottle, and dried at 120° vacuum for 1 h, and then argon is introduced to protect the glass bottle. The dried sample was then mixed with 2 mL of oleic acid and 1mmol of cis-oleic primary amine. When the temperature was also controlled at 150°, 0.5 mL of cesium oleate solution was added, stirred and reacted fully, and then mixed and reacted rapidly under the protection of nitrogen. Finally, the solution of $CsPbBr_3$ quantum dots was obtained by rapid cooling in the ice bath.

In addition, we used lanthanum oleate and lead bromide as precursors, then used hot injection method and fast ion exchange technology for inert gas protection. The $CsPbBr_3$ quantum dots were synthesized by reaction in the oil phase. After centrifugation and purification by high-speed centrifuge, a total inorganic metal $CsPbBr_3$ quantum dot solution with a concentration of 10 mg/mL and emitting green fluorescence was prepared using n-hexane as solvent. The porous Si/TiO_2 substrate was ultrasonically cleaned with absolute ethanol and deionized water for 15 min, dried by a nitrogen gun and then placed in a drying oven at 80° for 30 min; the prepared quantum dot solution was uniformly stirred by a magnetic stirrer to obtain a yellow transparent $CsPbBr_3$ quantum dot spin-coating solution. The obtained quantum dot spin-coating solution was dropped onto the porous Si/TiO_2 substrate by a special syringe using a one-step spin coating method. The homogenizing speed was maintained at 900 r/min for 5–10 s before dripping, the homogenization speed of 3500 r/min was maintained for 10–20 s after the dripping, at last a uniformly translucent $CsPbBr_3$ quantum dot film was obtained by spin coating. The amount of syringe droplets is determined by means of a microelectronic analytical balance with a reading accuracy of 0.01 mg. The experiment shows that the higher the spin coating speed, the longer the gelling time and the thinner the quantum dot film thickness.

The X-ray diffraction pattern of the $CsPbBr_3$ quantum dot is shown in Fig. 7. The characteristic

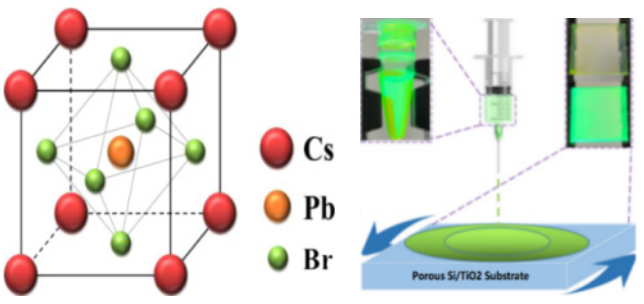

Fig. 6. $CsPbBr_3$ crystal structure and spin coating preparation process.

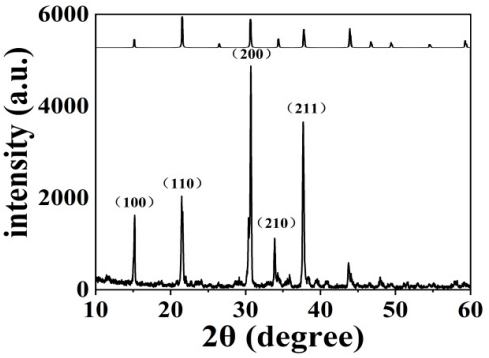

Fig. 7. $CsPbBr_3$ quantum dot XRD patter.

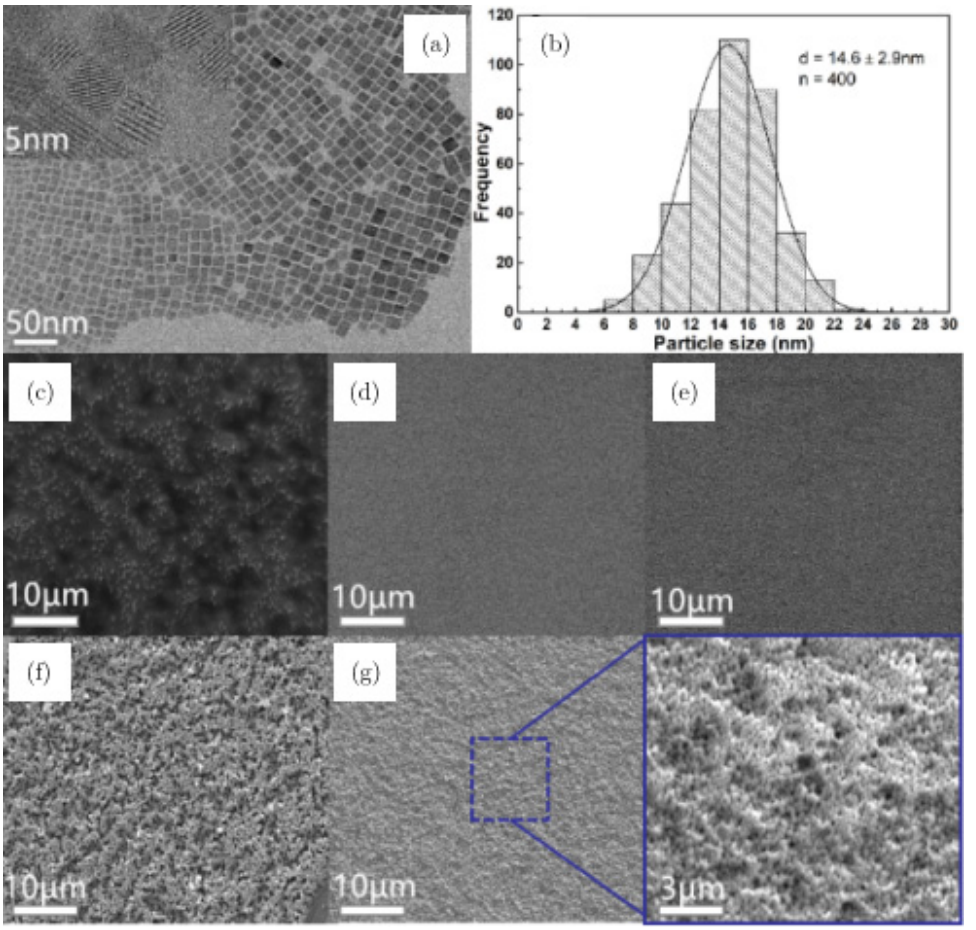

Fig. 8. (a) Transmission electron microscopy characterization; (b) Particle size distribution; (c)–(g) Scanning electron microscopy characterization of films with film thicknesses of 300, 450, 800, 1800 and 4500 nm, respectively.

peaks are 15.1°, 21.5°, 30.4°, 34.2° and 37.6°, respectively corresponding to the crystal structure {001}, {110}, {002}, {210}, {211}, which is consistent with the standard diffraction pattern obtained from the JCPDS database (No. 01-072-7929) and belongs to a cubic crystal structure. So, it belongs to the cubic crystal structure. In addition, we used TEM to perform characterization of $CsPbBr_3$ nanocrystals. Figure 8(a) shows the effect of $CsPbBr_3$ nanocrystals used in this paper. Figure 8(b) shows the nanocrystal size distribution map showing that the average crystallite size is about 15 nm. Figures 8(c) and 8(d) represent SEM images of $CsPbBr_3$ quantum dot films with different spin-on thicknesses, respectively.

5. Spectral Characterization of 3D Random Cavity

In summary, we have successfully fabricated a 3D random cavity device based on porous Si/TiO_2 nanowires. We grow TiO_2 nanowires on porous Si to form a 3D resonant cavity. A perovskite quantum dot is spin-coated on the surface of the 3D resonant cavity to form a distinguished 3D complex film. The specific structure diagram and overall characterization effect are shown in Figs. 9 and 10.

The thickness of the initial silicon substrate is $525 \pm 25\,\mu$m. However, in the etching process, the etching direction of silver particles is random, which effectively deepens the surface roughness of the substrate. Therefore, the thickness of porous silicon samples should be distributed in a range. As shown in Fig. 3, the surface of the sample 1-3 is the roughest, and its main corrosion depth ranges from $3\,\mu$m to $15\,\mu$m. In addition, as shown in the small figure in Fig. 10, nanowires of the order of 1 micron in length were grown in the gap of the rough surface. Finally, according to the mechanism of perovskite quantum dot optically pumped luminescence, increasing the surface roughness of the composite film

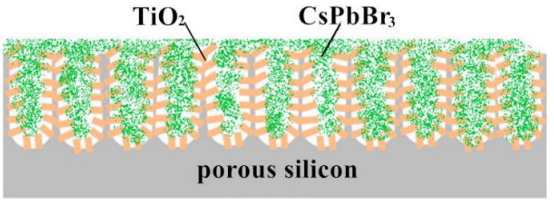

Fig. 9. 3D complex film schematic.

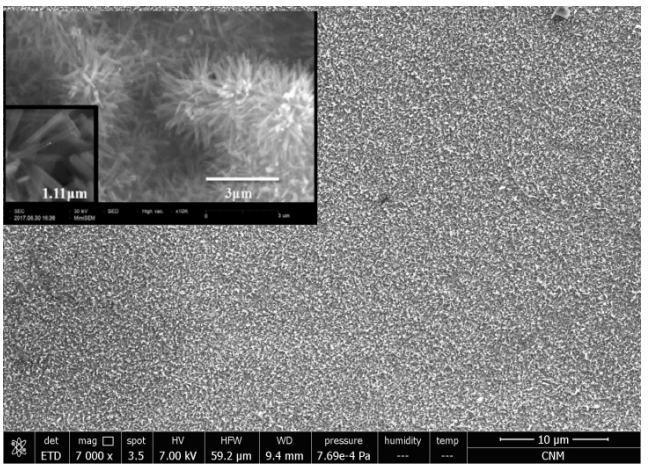

Fig. 10. 3D complex film overall characterization.

will directly increase the probability of photon coherent superposition and random lasing. Therefore, the thickness of $CsPbBr_3$ quantum dot thin films prepared by spin-coating method is also at a large dynamic range. We think that the thickness of spin-coated $CsPbBr_3$ quantum dot films will be randomly distributed from 300 nm to several microns according to different size, properties, depth and morphology of micropores. The overall effect of the coated complex film is shown in Fig. 10. In addition, in order to describe the spin coating effect of $CsPbBr_3$ quantum dot films from 300 nm to several microns, we describe and characterize them in Fig. 8.

In order to characterize the lasing enhancement ability of the complex film structure, we used the SD1220-V spectrometer of OTO Photonics Company with the resolution of 0.38 nm to carry out the following characterization experiments: firstly, $CsPbBr_3$ quantum dot films without resonator substrate were directly excited by continuous ultraviolet light with a wavelength of 365 nm. The spectra obtained at different excitation light power densities are shown in Fig. 11. It can be seen from the figure that the emission peak is at 520 nm and the FWHM is 20 nm. Subsequently, we excited the

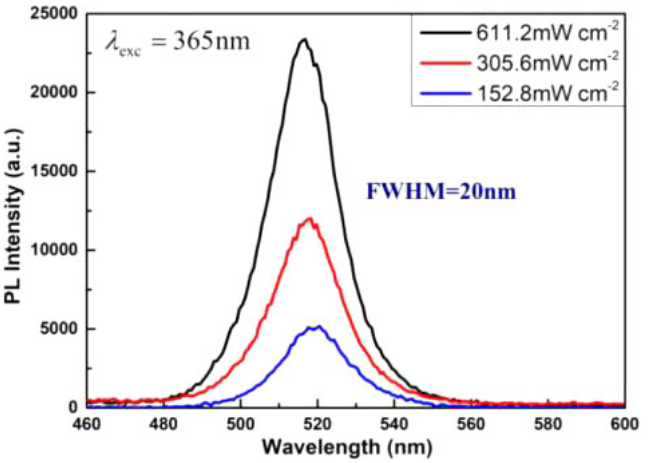

Fig. 11. Photoluminescence spectrum of $CsPbBr_3$ quantum dot film.

$CsPbBr_3$ quantum dot film with a 3D cavity substrate by the same continuous ultraviolet light, and its lasing spectrum is shown in Fig. 12.

It can be seen that the 2D porous Si surface structure (according to Fig. 3.) greatly increases the roughness of the surface of the quantum dots, and the 1D TiO_2 nanowires grown on the inner wall of the porous Si pores (according to Fig. 4.) greatly increase the fluorescence of $CsPbBr_3$. The probability of coherence in space finally achieves a random lasing under continuous ultraviolet light pumping.

The contrast effect is shown in Table 3. By comparing the continuous electron beam pumping lasing parameters published by our team in the previous period, the FWHM of the lasing peaks of

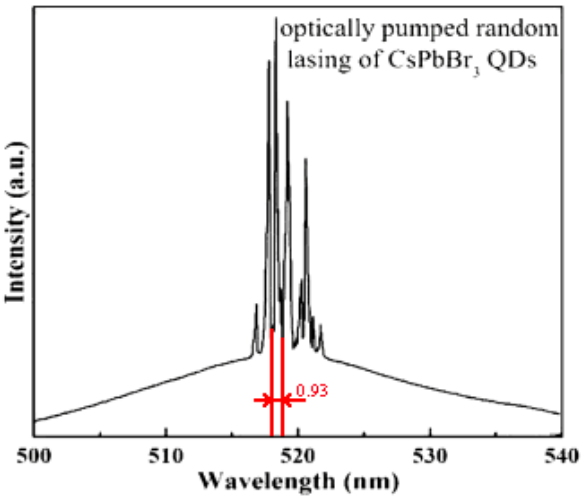

Fig. 12. Optically pumped spectrum of $CsPbBr_3$ quantum dot film with a 3D cavity substrate.

Table 3. Comparison of parameters between continuous electron beam pumping and optically pumping.[13]

Material	Geometry	Pump model	Threshold	FWHM
$CsPbBr_3$	Film/ITO	CW/EB Pump	$3.4\,mW/cm^2$	0.9 nm
$CsPbBr_3$	Porous Si/NW	CW/optically pump	$305\,mW/cm^2$	0.93 nm

both are relatively similar, and the overall lasing effect is similar.

Although the lasing threshold of the perovskite quantum dot films pumped by continuous electron beam is very low, the 3D resonant cavity structure proposed in this paper can avoid the restriction of vacuum environment on electron beam pumping, which immediately leads to more flexible applications. In addition, our team will further study the lasing threshold and luminescence characteristics of the 3D resonant cavity structure under the condition of electron beam pumping.

6. Conclusion and Outlook

In summary, the porous Si/TiO_2 nanowire 3D random cavity device structure proposed in this paper can completely achieve random lasing of perovskite quantum dots under continuous optical pumping. At the same time, the 3D resonant cavity has the advantages of high chemical stability and low manufacturing cost. Our team will further introduce the 3D cavity structure into the perovskite quantum dot electrical injection device in the future. If the structure can achieve random lasing of perovskite LEDs, it will provide important support for the development of information optics.

Acknowledgments

This work was funded by the National Natural Science Foundation of China (Nos. 51602028, 61905026, 11874091 and 51502023) and the Jilin Province Science and Technology Development Plan Project Number (No. 20180519019JH).

References

1. K.-H. Lee *et al.*, *ACS Nano* **11**, 10941 (2015).
2. J. Dai *et al.*, *Appl. Phys. Lett.* **99**, 063112 (2011).
3. V. L. Colvin, M. C. Schlamp and A. P. Alivisatos, *Nature* **370**, 354 (1994).
4. W. K. Bae, J. Kwak, J. Lim, D. Lee and S. Lee, *Nano Lett.* **10**, 2368 (2010).
5. K. H. Lee *et al.*, *ACS Nano* **8**, 4893 (2014).
6. Y. Cao *et al.*, *Nature* **249**, 652 (2018).
7. L. Protesescu *et al.*, *Nano Lett.* **15**, 3692 (2015).
8. C. Motta, F. El-Mellouhi and S. Sanvito, *Sci. Rep.* **5**, 12746 (2015).
9. K. Wang, S. Sun, Ch. Zhang, W. Sun, Z. Gu, S. Xiao and Q. Song, *Mater. Chem. Front.* **1**, 447 (2017).
10. Z. Qitao, P. J. Gyu, N. Riming, T. A. Kumar, H. Dogyeong, P. Jing, S. Sang Il and K. Taesung, *ACS Nano* **12**, 8406 (2018).
11. L. Dou *et al.*, *Proc. Natl. Acad. Sci.* **114**, 201703860 (2017).
12. P. Perumal, C. Wang, K. Boopathi, G. Haider, W. Liao and Y. Chen, *ACS Photonic* **4**, 146 (2017).
13. F. Haibo *et al.*, *Chin. Opt. Lett.* **18**, 230 (2020).
14. A. Safdar, Y. Wang and T. Krauss, *Opt. Express* **26**, A75 (2018).
15. J. Song, J. Li, X. Li, L. Xu, Y. Dong and H. Zeng, *Adv. Mater.* **27**, 7161 (2015).
16. Y. Wang, X. Li, J. Song, L. Xiao, H. Zeng and H. Sun, *Adv. Mater.* **27**, 7101 (2015).
17. S. Yakunin, L. Protesescu, F. Krieg, M. Bodnarchuk, G. Nedelcu, M. Humer, G. Luca, M. Fiebig, W. Heiss and M. Kovalenko, *Nat. Commun.* **6**, 8056 (2015).
18. T. Chiba *et al.*, *Nat. Photonics* **512**, 681 (2018).
19. K. Lin *et al.*, *Nature* **562**, 245 (2018).
20. L. Cunlong, Z. Zhigang, H. Ceng, H. Zhiping, T. Xiaosheng, D. Juan, L. Yuxin and S. Kuan, *Nano Energy* **40**, 195 (2017).
21. Y. Dongdong, S. Tongchao, Z. Zhigang, Z. Tingwei, L. Zhengzheng, Z. Zeyu, D. Juan, L. Yuxin and T. Xiaosheng, *SMALL* **23**, 1901173 (2019).
22. L. Cunlong, H. Ceng, Z. Yubo, Z. Zhigang, W. Ming, T. Xiaosheng and D. Jihe, *Solar Energy Mater. Solar Cells* **172**, 341 (2017).
23. L. Xiangming, X. Tao, L. Yulong, Z. Zhigang, P. Xiaoshi, W. Huiyue, Z. Weiyi and W. Feng, *Solar Energy Mater. Solar Cells* **187**, 249 (2018).
24. L. Cunlong, Z. Zhigang, C. Weiwei, H. Zhiping, T. Xiaosheng, H. Wei, S. Kuan, L. Xianming and C. Weimin, *Opt. Express* **13**, 15071 (2016).
25. Z. P. Huang and N. Geyer, *Adv. Mater.* **23**, 285 (2011).
26. P. Perumal, C. Wang, K. Boopathi, G. Haider, W. Liao and Y. Chen, *ACS Photonics* **146**, 4 (2017).
27. S. Eaton, M. Lai, N. Gibson, A. Wong, L. Dou, J. Ma, L. Wang, S. Leone and P. Yang, *Proc. Natl. Acad. Sci.* **1993**, 113 (2016).